Geomorphology 250 (2015) 53–62

Contents lists available at ScienceDirect

Geomorphology

journal homepage: www.elsevier.com/locate/geomorph

Impact of consecutive extreme rainstorm events on particle transport: Case study in a Sonoran Desert range, western USA

Ronald I. Dorn

School of Geographical Sciences & Urban Planning, Arizona State University, Tempe, AZ 85287-5302, USA

ARTICLE INFO

Article history:
Received 23 April 2015
Received in revised form 23 August 2015
Accepted 24 August 2015
Available online 1 September 2015

Keywords:
Desert geomorphology
Erosion rate
Overland flow
Threshold

ABSTRACT

Quantifying erosion rates in different landscape settings provides insight into how landforms change under different climatic, tectonic and anthropogenic influences. Sediment traps designed to capture grus detached from granitic hill crests of an arid Sonoran Desert mountain range were placed prior to every precipitation event over a three-year period, just above rills that drain areas between 18 and 68 m^2. The slopes are underlain by moderately to strongly weathered granitic rocks to a depth of about a meter. Within this 3-year window, a 1000-year precipitation event followed 27 days later by a 500-year event detached granitic grus in amounts far greater than previous storms, capturing between 22× and 63× the average amount transported in the previous 59 rain events — indicating the non-linear nature of the response of grus detachment to precipitation intensity. Considering every precipitation event over a 3-year period, no detachment occurred from events with less than 2 mm of total rainfall, and only minimal erosion occurred from rainfall events with totals between 2 and 10 mm with durations typically less than 30 min. Detachment increased greatly with rain intensities of 36 mm/h or more. Grus detachment from these arid crests increases with drainage area, a higher percentage of exposed soil, and steeper slopes. $^{87}Sr/^{86}Sr$ ratios reveal that suspended sediment transported from hill crest to trap derives from recycled dust and not the local granite bedrock.

1. Introduction

Developing a better understanding of processes and rates of soil particle erosion remains an important part of geomorphology research, with considerable progress made recently (Garcia-Ruiz et al., 2015). Still, relatively few studies exist for arid slopes (Crouvi et al., 2015) and even fewer along the crests of arid ranges. Thus, this project commenced in 2011 to gather data on detachment of particles from arid granitic crests during every precipitation event. Fortuitously, the end of the three-year study included two extreme storms 27 days apart at South Mountain, a Sonoran Desert range surrounded by metropolitan Phoenix, Arizona. During the 2014 Arizona summer monsoon season, a 1000-year precipitation thunderstorm event took place on August 12, followed by a longer-duration 500-year soaking by hurricane moisture on September 8, 2014.

Extreme rainstorms shed light on earth surface processes that shape arid and semi-arid landforms (Lekach and Schick, 1983; Schick, 1988; Pickup, 1991; Shaw et al., 1992; Dick et al., 1997; Coppus and Imeson, 2002; David-Novak et al., 2004; Mather and Hartley, 2005; Harvey, 2006; Moharana and Kar, 2010), for example in highlighting the importance of soil and vegetation conditions (Osterkamp and Friedman, 2000) or in emphasizing the importance of runoff coefficients (Puigdefabregas et al., 1998). Given the relative paucity of geomorphic data associated with extreme desert rains, value exists in a realistic research practice (Richards et al., 1995) linking the properties of a field area to insights obtained through unique observations.

The focus of this paper rests in reporting and analyzing basic field observations on grus detachment events in response to regular precipitation events and also to extreme rainstorms on desert slopes. The field area section of this paper sets the stage. The methods section then outlines: (a) gathering 3 years of data on grus detachment near interfluves; (b) analyzing granitic decay near sediment trap sites through electron microscopy; and (c) determining stable strontium-isotope ratios to differentiate *in situ* detachment of rock material from eolian dust. The results and discussion sections explore how the geomorphic impact of consecutive extreme storms compare with less extreme precipitation events on arid granitic ridge crests.

2. Field area

South Mountain stretches approximately 29 km and forms a municipal preserve in Phoenix, Arizona, USA. The study area is in the eastern portion and consists of mid-Tertiary granitic rock types (Fig. 1). Metamorphic core complexes such as South Mountain in Arizona formed concurrently with upper crustal extension from the release of compressional stress after the Mesozoic Sevier and Laramide Orogenies (Nations and Stump, 1981; Coney and Harms, 1984; Holt

E-mail address: ronald.dorn@asu.edu.

http://dx.doi.org/10.1016/j.geomorph.2015.08.017
0169-555X/

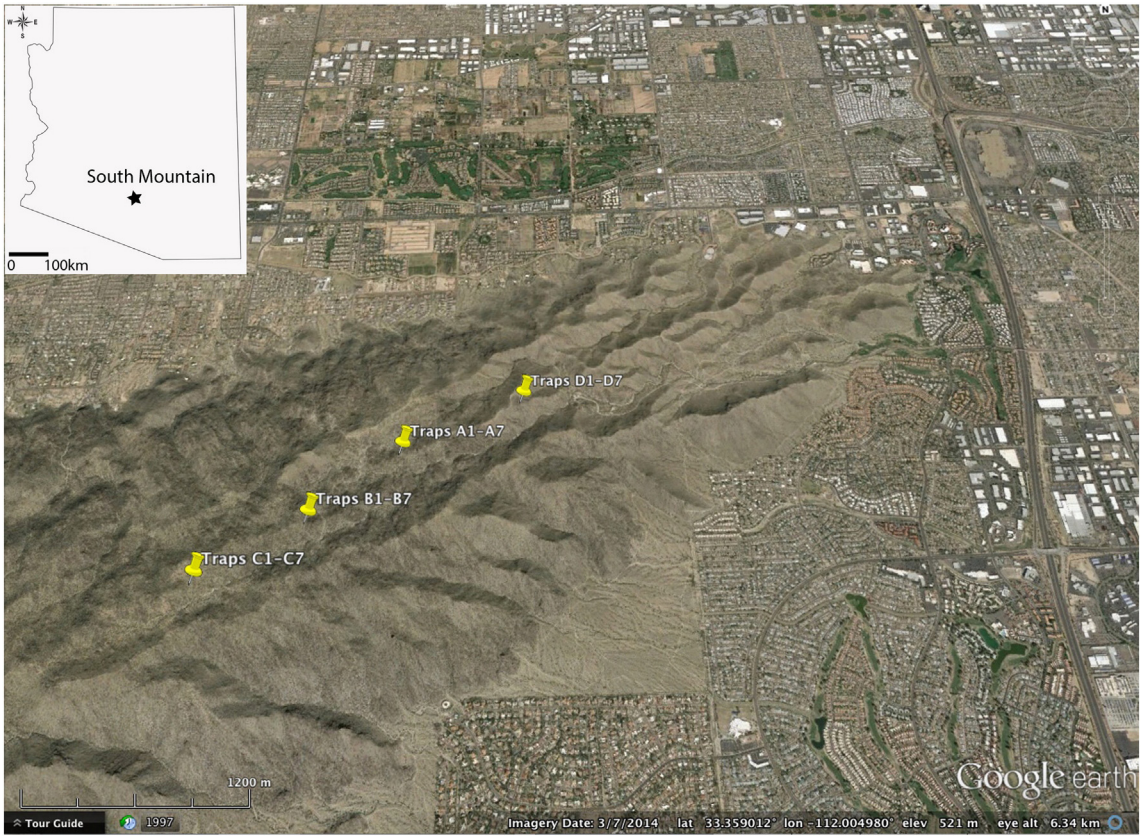

Fig. 1. The 28 sediment traps are distributed across four study ridge crests within South Mountain. These are in the eastern half of South Mountain in Tertiary granitic rock types. The base image from 2014 is used following permission guidelines for Google Earth [http://www.google.com/permissions/geoguidelines.html].

et al., 1986). South Mountain's uplift ended ~8–14 Ma ago (Spencer, 1984; Reynolds, 1985).

The climate and vegetation of South Mountain represent the rest of the Sonoran Desert in central Arizona. Annual precipitation averaging 208 mm splits evenly between summer and winter maxima (Climate Office of Arizona, https://azclimate.asu.edu/climate/climate-of-phoenix-summary/). Winter rainfall derives from Pacific cold fronts and low-pressure systems. Moist air masses from the Gulfs of Mexico and California, combined with surface heating and upper level tropospheric disturbances, generate summer thunderstorms during the July–September Monsoon season that sometimes extends into October from Pacific hurricane moisture.

Sonoran Desert trees grow along ephemeral washes and on hillslopes where overland flow concentrates, including palo verde (*Parkinsonia microphylla*), ironwood (*Olneya tesota*), and elephant trees (*Bursera microphylla*). Desert scrub vegetation found on slopes includes creosote bush (*Larrea tridentata*), brittlebush (*Encelia farinosa*), triangle-leaf bursage (*Ambrosia deltoidea*), catclaw acacia (*Acacia greggii*), desert globe mallow (*Sphaeralcia ambigua*), and ocotillo (*Fouquieria splendens*). Hillslopes also host succulents such as saguaro (*Carnegiea gigantea*), barrel (*Ferocactus cylindraceus*) and hedgehog (*Echniocereus engelmannii*) cactus.

Detachment of granitic grus from bedrock exposures limit erosion rates in the eastern half of South Mountain that is composed of granitic lithologies (Fig. 2A, B). Granitic slopes mix decayed bedrock, relatively fresh bedrock with kopje (Twidale, 1982) forms, tors and detached granitic grus to create a landscape of irregularly-shaped steep bedrock slopes and smoother grus-covered forms that are less steep (Fig. 2A, B). A slope map (Fig. 3) sheds additional light on granitic landforms; in the granitic eastern half of South Mountain, slopes steeper than 23% provide a proxy for the location of granitic bedrock that is detachment limited. In contrast, grus transport dominates on slopes lower than ~23%. A working hypothesis is that these grus-dominated slopes are underlain by granitic rock that has undergone sufficient dissolution and alteration in the subsurface to not be in a detachment-limited condition. Since the sediment traps were placed in zones of already detached granite, a component of this research assesses the working hypothesis of subsurface weathering.

3. Extreme rain events

An August 12, 2014 1000-year precipitation event occurred when Mexican monsoon moisture "juiced" the atmosphere over Arizona, with the triggering mechanism being an upper-level inverted trough moving into the area from Baja California. For the August 12 event, the Arizona State Climatologist's rain gage at South Mountain measured 26 mm in 10 min, 68 mm in 50 min and 86 mm in 100 min translating into intensities of 154, 81, and 51 mm/h or a 200-year, 500 ± year, and 1000 ± year event (Dr. Nancy Selover, Arizona State Climatologist, personal communication, 2014). Radar reveals South Mountain to have been the focus of the most intense precipitation that took place over time span of less than 2 h.

The September 8, 2014 event contrasted greatly in that remnant moisture from eastern Pacific Hurricane Norbert moved over the entire south-central portion of Arizona, leading to precipitation lasting over 4 h and generating even more rain for South Mountain than the August 12th thunderstorm complex. The event started with 36 mm in 25 min (87 mm/h). Another 68 mm then soaked the range over the next 285 min (14 mm/h) where precipitation intensities occasionally exceeded 30 mm/h, but only for 5 min at a time. Other rain gages across South Mountain reflect these amounts and intensities. Taken as an entire event, the September 8 storm produced the wettest day on record in Phoenix, AZ, and it is considered a 500-year precipitation event by the U.S. National Weather Service.

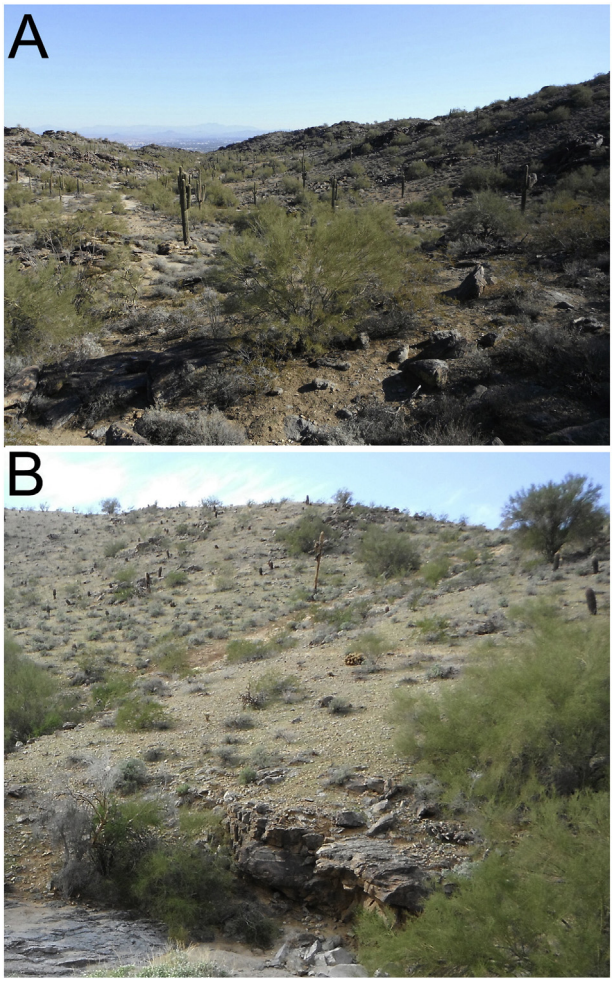

Fig. 2. Transport of grus by overland flow dominates slope processes in the granitic eastern portion of South Mountain. 4 m-tall saguaro (*Carnegiea gigantea*) columnar cacti in image A and 3 m-high paloverde (*Parkinsonia microphylla*) trees in image B provide a sense of scale.

While these two events do not represent the maximum precipitation that could be seen at South Mountain (Tomlinson et al., 2013), these two days alone brought more rain than the annual average precipitation. These storms triggered debris flows on the western gneissic slopes of South Mountain and detached abundant grus from granitic slopes in the eastern portion.

4. Methods

4.1. Strontium isotopes to assess nature of the suspended load

Dust transport and deposition occurs regularly in association with Arizona summer thunderstorms (Brazel, 1989; Marcus and Brazel, 1992). Because strontium isotopes have the potential to discriminate source materials (Capo et al., 1998; Capo and Chadwick, 1999), $^{87}Sr/^{86}Sr$ ratios were used to assess the hypothesis that the suspended sediment load coming into and out of the sediment traps derives from externally sourced dust and not from the granitic bedrock.

$^{87}Sr/^{86}Sr$ ratios were measured in the following types of samples: (a) winter precipitation; (b) summer precipitation; (c) dust from summer dust storms in 2013 and 2014; (d) the suspended sediment load exiting 3 traps; and (e) grus grains from those same 3 traps. The dust, suspended sediment, and trapped grus were separated into the acetic acid-soluble fraction that represents carbonate and labile Ca and the silicate fraction. Samples were normalized to the $^{87}Sr/^{86}Sr$ ratio of 0.1194 and compared to the Eimer and Amend standard (0.7080).

Winter precipitation samples 1, 2 and 3 were collected in a wide-mouth glass beaker from N 33.35606 W 112.01789 on 11/4/2011, 12/12/2011, and 12/13/2011. Summer precipitation samples 1, 2 and 3 were collected in a wide-mouth glass beaker from N 33.35606 W 112.01789 on 7/14/2012, 8/21/2012, and 8/23/2012. Dust samples were collected from this same area using a design adopted by the U.S. Geological Survey (Reheis and Kihl, 1995) and were collected at the end of July, August and September in 2012. Suspended sediment samples 1, 2 and 3 were collected from the outflow of three different sediment traps at this location.

4.2. Assessing the state of granitic decay

Detachment by overland flow requires that the bedrock granitic material be in a sufficient state of decay to allow soil production or stripping by the shear stress. Thus, in order to understand the state of decay of the bedrock along the studied ridge crests, three pits near the four sediment trap areas presented in the next section were dug to a depth of 1.0 m or until the pit could not be deepened by hand. Samples were also collected from kopje forms (Twidale, 1982) in order to compare the pit samples with fresh exposed bedrock in a detachment-limited state. In addition, notes were made on the weathering grade in the pits (fresh, slightly weathered, moderately weathered, highly weathered, completely weathered, residual soil) using Ehlen's (1999) rock classification material system.

Samples collected for electron microscope study were placed in epoxy and polished for examination with back-scattered (BSE) and secondary electrons. Using methods detailed previously (Dorn, 1995), digital image processing of BSE imagery at a scale of 1000× enables calculation porosity in rock material — in this case a cross-sectional area of 2 mm^2. The reported porosity includes intra-mineral pores and pores along mineral-grain boundaries. While porosity data are calculated to hundredths of a percent, a conservative solution in dealing with different pore types is to round off to the nearest tenth. These porosity data provide insight to the state of decay because greater internal porosity requires less shear stress to detach and erode grus (Ehlen and Wohl, 2002; Ehlen, 2005).

4.3. Traps to record detachment of grus

Four ridge crests in the granitic eastern section of South Mountain hosted 28 sediment traps, 7 for each ridge crest. Prior to determining the location of trap placement, pathways of water movement were observed during summer monsoon thunderstorms to identify trap locations just above where rilling initiates. For a period of 3 years, sediment traps were placed prior to every predicted precipitation event starting in October of 2011. Since summer monsoon precipitation is often difficult to predict with accuracy, summer traps were placed regularly and removed after every precipitation event recorded by the nearest automated rain gage. Trap placement was discontinued after September of 2014 — ending with a record of grus detachment and transport for a 3-year period.

Traps placed during the winter consist of a rectangular solid shape that is hollowed in the middle with a length of about 13 cm and openings on both ends of 22 cm^2. Fig. 4 illustrates a brown-colored trap at a typical trap setting. Trap mouths have sloped openings that allows water and sediment to go in, but only water and suspended load to exit. For the summer monsoon, larger traps were placed — but with a similar geometry of an open-ended rectangular shape with an upraised lower end to prevent bedload from escaping. The maximum capacity of these traps was not exceeded, but the trap efficiency is limited to only bedload, since suspended load and dissolved load left the traps.

Each of the 28 traps records grus detachment and transport from positions only a few meters from ridge crests, with areas between 18 and

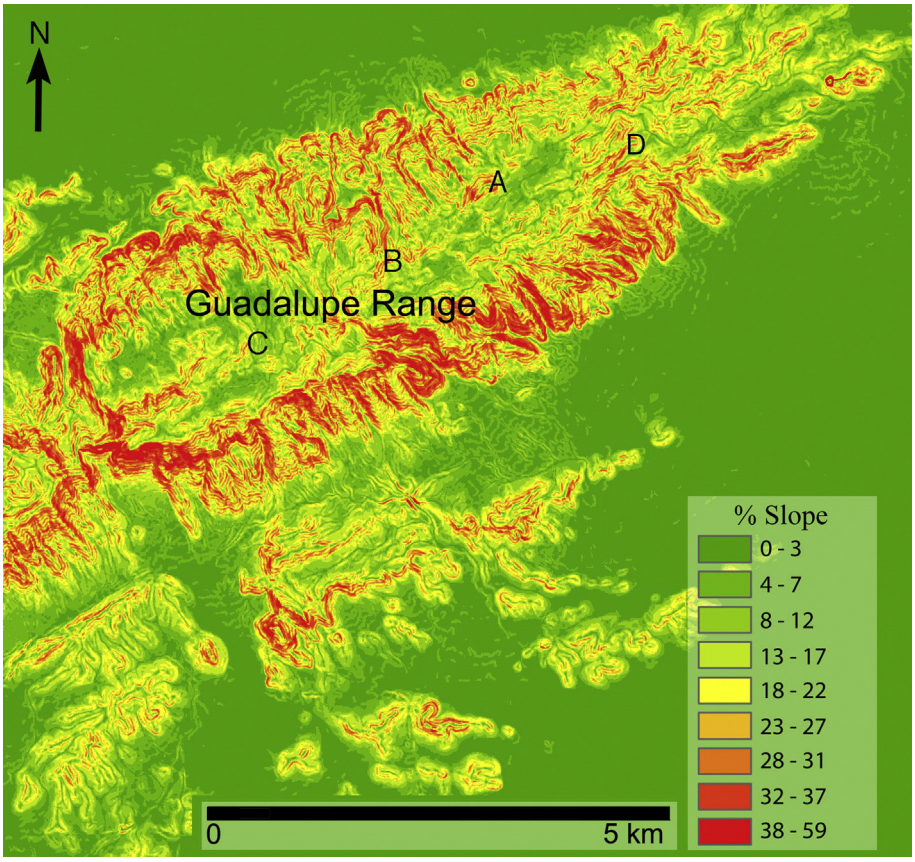

Fig. 3. Slope map of the granitic eastern portion of South Mountain, identifying the four ridges hosting sediment trap site A1–7. B1–7, C1–7, and D1–7. Slopes steeper than 23% in the granitic Guadalupe Range identify exposures of bedrock, and grus cover mixed with boulders and cobbles dominates lesser slopes.

Fig. 4. Typical detachment trap setting very near the crest. Note that the typical armoring by cobbles, boulders and bedrock. Each trap (brown rectangular box) was either attached to a large clast on its underside by superglue, but a few were weighted down with clasts placed inside and then removed after trap collection. A sense of scale is provided by the triangle-leaf bursage (*Ambrosia deltoidea*) plants in the middle of the frame are 0.5 m high.

Table 1
$^{87}Sr/^{86}Sr$ ratios of precipitation, dust and transported sediment collected at South Mountain, Arizona.

Sample	Sample 1	Sample 2	Sample 3
Winter precipitation	0.7100	0.7102	0.7105
Summer precipitation	0.7111	0.7113	0.7116
Dust leachate from summer 2013	0.7088	0.7075	0.7083
Dust leachate from summer 2014	0.7075	0.7072	0.7080
Suspended sediment leachate	0.7073	0.7069	0.7077
Dust silicate from summer 2013	0.7110	0.7115	0.7123
Dust silicate from summer 2014	0.7108	0.7112	0.7116
Suspended sediment silicate fraction	0.7111	0.7115	0.7118
Leachate of grus grains	0.7133	0.7136	0.7122
Grus grains after leaching	0.7233	0.7250	0.7144

68 m^2. The reason for such small drainages is an attempt to capture grus being detached from ridge crests, whether by raindrops (Furbish et al., 2009) or rain-impacted flow (Parsons et al., 1998), and then transported a few meters by the inter rill overland flow (Parsons et al., 1991). Field observations during intense rainstorms indicated that these traps captured grus detached by rainsplash and moved short distances by subsequent overland flow. While detachment rarely occurred from boulder surfaces, qualitative field observations reveal that almost all detachment took place on the sandy surfaces between cobbles and boulders (Fig. 4). After each precipitation (rain) event, accumulated grus was oven dried at 100 °C, weighed, and sieved to calculate the D_{50} or median grain size of the grain-size distribution of the material in the trap.

For each trap drainage area, measurements at 10 slope positions generated an average slope. Three different types of surfaces exist in each trap drainage area: % perennial plant canopy; % exposed bedrock; and % soil exposed. The area of the perennial plant canopy and exposed bedrock were measured in the field using a 1 m × 1 m square gridded to decimeters that was moved over each study area, but % exposed soil was calculated by subtracting canopy and bedrock cover from 100%.

5. Results

5.1. Strontium isotopes to assess nature of the suspended load

$^{87}Sr/^{86}Sr$ ratios presented in Table 1 indicate a common source for the leachate fraction of the summer dust and the suspended sediment exiting the traps, where leachate records the carbonate and labile Ca (Capo et al., 1998). Similarly, $^{87}Sr/^{86}Sr$ ratios reveal a common source for the silicate fraction of summer dust and suspended sediment. The grus grains collected from the sediment traps, in contrast, host a very different strontium isotope signal, and the leachate coming out of grus grains appears to reflect a mix of the granitic grus signal and the dust silicate signal. Taken in total, these findings are consistent with the hypothesis that the suspended sediment load flowing out of the traps derives mostly from dust and not from the granitic bedrock.

5.2. Assessing the state of granitic decay

Electron microscope samples collected from pit depths (Table 2) between 0.7 m and 1.0 m reveal that at least two sets of processes play a role in decaying the upper meter of the field sites into a sufficient state of grussification to permit detachment. The least decayed samples portrayed in Fig. 5A–D show the importance of biotite hydration and oxidation to generate cracking that breaks apart the cohesion of interlocking minerals. These cracks facilitate water transport that enhances mineral porosity, as shown in Fig. 5E. Table 2 presents quantitative data on the state of decay of the granitic rock, as reflected in percent porosity, before it reaches the surface and is exposed to overland flow.

These findings reveal that the granitic materials underlying the studied ridge crests and slopes are not detachment limited, at least not until the upper meter. Instead, subsurface decay effectively prepared the granitic rock for detachment. Erosion of the grussified granite is, thus, limited by precipitation amounts and subsequent overland flow. The results presented in the next section reflect precipitation acting on 28 drainage areas underlain by decayed granite and not detachment-limited slopes.

5.3. Traps to record detachment of grus

The online supplementary file (link to file here) presents data tables on the granitic grus collected in the 28 sediment traps. These tables record the grams of bedload trapped in every precipitation event. This supplementary file includes data on: drainage area, average slope, percent perennial canopy, percent soil exposed, percent exposed bedrock, and D_{50} particle size for each trap.

These data record detachment at and near drainage divides. Field observations during precipitation events indicate that short-distance transportation of a few meters or less occurred from inter rill flow after detachment (Parsons et al., 1991). Direct observations of detachment did not involve high-speed photography, and thus a determination could not be made whether ejection was from raindrops (Erpul et al., 2005; Furbish et al., 2009) or rain-impacted flow (Parsons et al., 1998).

Table 2
Percent porosity of granitic materials in pits dug near sediment traps A1–7, B1–7, C1–7, and D1–7. Pits were dug to depths of 1 m or until pit digging was not possible by hand. Samples were also analyzed using Ehlen's (1999) rock material classification of weathering grade: fresh (F), slightly weathered (S) moderately weathered (M), highly weathered (H), completely weathered (C). Comparison samples were collected from nearby granitic kopjes.

Sample	Location	Percent porosity	Material grade
0.7 m A1–A7 — pit 1	N 33.35606 W 112.01789	22.3	M
1.0 m A1–A7 — pit 2	N 33.356207 W 112.017732	31.4	H
1.0 m A1–A7 — pit 3	N 33.356003 W 112.018075	40.1	C
0.9 m B1–B7 — pit 1	N 33.35142 W 112.02399	33.0	H
0.9 m B1–B7 — pit 2	N 33.351326 W 112.024602	34.2	H
0.9 m B1–B7 — pit 3	N 33.351075 W 112.025342	43.0	C
0.7 m C1–C7 — pit 1	N 33.34771 W 112.03091	25.1	M
1.0 m C1–C7 — pit 2	N 33.347710 W 112.030910	30.9	H
1.0 m C1–C7 — pit 3	N 33.347329 W 112.031672	31.0	H
1.0 m D1–D7 — pit 1	N 33.35984 W 112.00908	39.3	C
1.0 m D1–D7 — pit 2	N 33.360212 W 112.008104	32.2	H
1.0 m D1–D7 — pit 3	N 33.359468 W 112.009477	42.5	C
Granitic Kopje 1	N 33.35624 W 112.018998	3.4	F
Granitic Kopje 2	N 33.357278 W 112.016396	4.2	F
Granitic Kopje 3	N 33.351658 W 112.023159	2.3	F
Granitic Kopje 4	N 33.346996 W 112.031116	9.4	S
Granitic Kopje 5	N 33.358247 W 112.012154	5.0	F

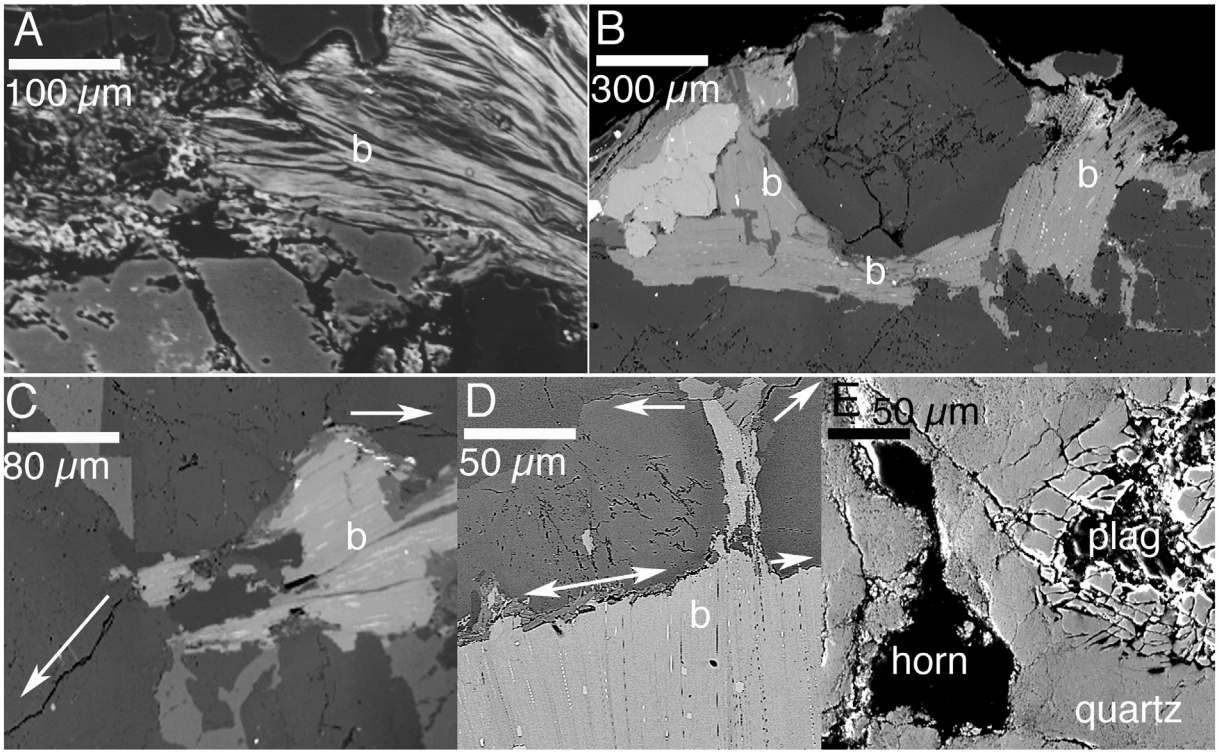

Fig. 5. Biotite (letter b) hydration and oxidation fractures minerals and grain boundaries to produce grus. Oxidation of biotite (b) produces the bright spots of iron oxidation seen in the biotite. Arrows in images C and D show crack propagation that begins enhances water flow and grussification. Hydration produces splitting best seen in image A. Image A also illustrates how biotite hydration can fracture the surrounding minerals. Image B biotite decay on three sides of a plagioclase grain that produces a series of internal fractures. In addition to biotite decay, dissolution of minerals such as hornblende and plagioclase in image E leads to fragmentation of minerals (especially hornblende, plagioclase) and collapse of the structure of interlocking minerals. BSE images show atomic number imaged A–D, and secondary electrons imaged in E show topography. Scale bars are in micrometers.

Considered as a whole, data from the 28 collection traps reveal that a higher percentage of exposed soil, larger drainage areas, and steeper slopes all enhance grus detachment and subsequent transportation into the traps (Fig. 6). The following multiple regression with an adjusted R^2 of 0.79 is statistically significant ($p < 0.001$):

$$g = -2559 + 64\,Ad + 690\,Sl + 2.1\,So \quad (1)$$

where g is yearly average in grams and the standardized regression weights are 0.591 (Ad, or drainage area), 0.8609 (Sl, or average slope), and 0.0159 (So, or percent of soil exposed). In contrast, the D_{50} shows no relationship to the annual average of trapped grus.

A plot of grus detached and transported during each precipitation event (Fig. 7) reveals that no transport took place during rains of 2 mm or less. Only some transport (less than 100 g) took place during

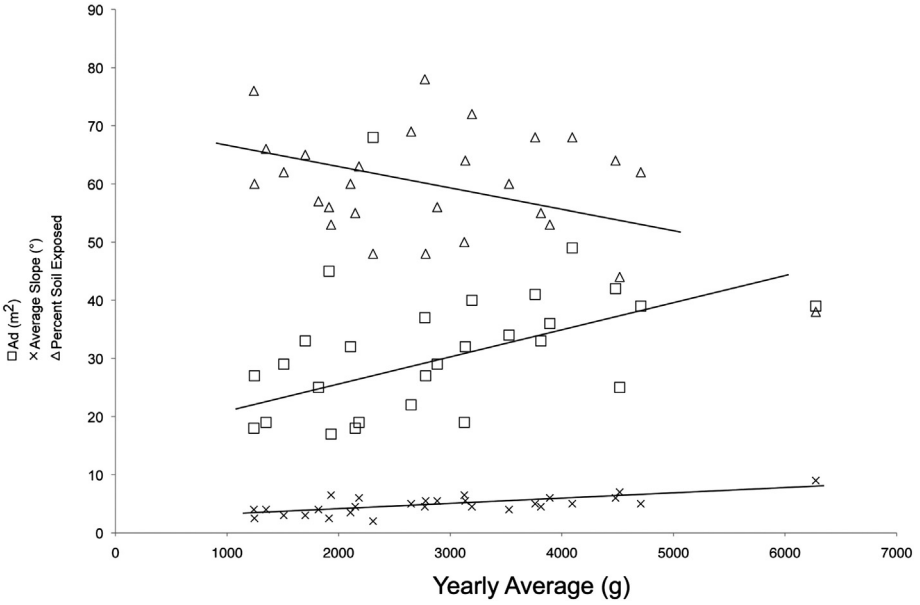

Fig. 6. Scattergraph (with linear regressions) of relationships between the average grams of detached grus and the drainage areas, average slopes, and percent soil exposed in the 28 catchments. Pearson correlation between the yearly average and percent soil exposed (−0.349), average slope (0.701), and drainage area (0.367) reflect the strength of each separate relationship.

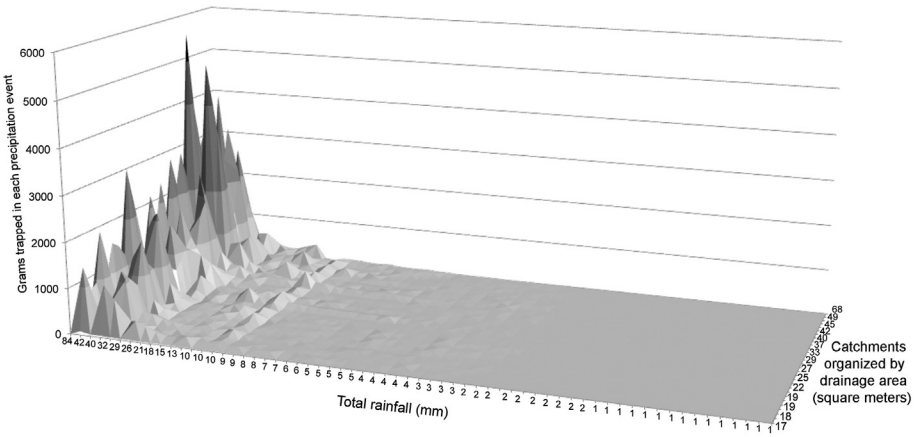

Fig. 7. Plot of grams trapped for precipitation events over a 3-year period. Repetition of rainfall and catchment drainage occurs, because this graph shows every single precipitation event. The shorter axis showing the 28 traps is ordered by drainage area in m^2. The longer axis indicating total rainfall amount is also an ordinal plot.

precipitation events totaling less than 10 mm. Only eleven rains totaled more than a centimeter, and these few events transported several hundred grams or more. Total rainfall amounts, however do not inform on the importance of intensity.

The large jump in detachment appears to be associated with precipitation intensities of 36 mm/h or more as seen in Fig. 8, where every precipitation event with intensities of 4 mm/h is plotted and organized by catchment area. While drainage area also promotes grain detachment and transport to traps, the sudden jump at 18 mm/30 min occurs in drainages of all sizes.

6. Discussion

6.1. Mode switching

Mode switching in geomorphic systems involves a variety of geomorphic processes and scales as well as increases or decreases in rates of change (Phillips, 2014). In this case of the resistance of arid granitic hill crests to erosion (detachment and then transport to rills), mode switching appears to be controlled by precipitation intensity as viewed from the perspective of 3 years of record (Fig. 8).

A record of less than 3 years is generally considered less than optimal (Garcia-Ruiz et al., 2015); however, the inclusion of two extreme events in the data set makes these observations meaningful. The sum of all of the masses detached and transported by just three events with the most intense precipitation (Aug 21, 2012, Aug 12, 2014, and September 8, 2014) equaled or exceeded the mass transported by all of the other events combined. The ratio of these top 3 events to all of the other events combined averaged 1.79 with a standard deviation of 0.54 for the 28 catchments. These large events indicate the power of a mode switch.

Consider one anecdotal observation related to the August 12, 2012 extreme event of 39.1 mm of total precipitation with a 21.8 mm/30 min maximum intensity. A grain of grus was collected after direct observation of detachment from decayed bedrock. Fig. 9 shows electron microscope textures associated with this detachment: a texture of slightly sheared grains could have been produced by the mechanical action of detachment; and a pre-condition of thorough mineral decay appears to be associated with grain detachment resulting from the force of intense rain.

As Phillips (2014: 76) writes: "the way we understand these mode switches also profoundly influences applied geomorphology and environmental management." Using Fig. 9 as a thought exercise, *in situ* mineral decay takes place along ridge crests as the normal long-term process, generating the inter-grain porosity and clay mineral transformation seen in Fig. 5 and Table 2. Only the most extreme precipitation events interrupt this normative condition, when geomorphic activity along ridge crests switches modes to detachment and particle transport. Phillips' (2014) concern over management is warranted even in this arid setting, because there is a definite tendency of preserve managers to go in and "fix" erosion associated with extreme storms; this tendency should be tempered by the realization of the rarity of these mode switches. Rilling in this arid setting will be filled-in slowly by lower

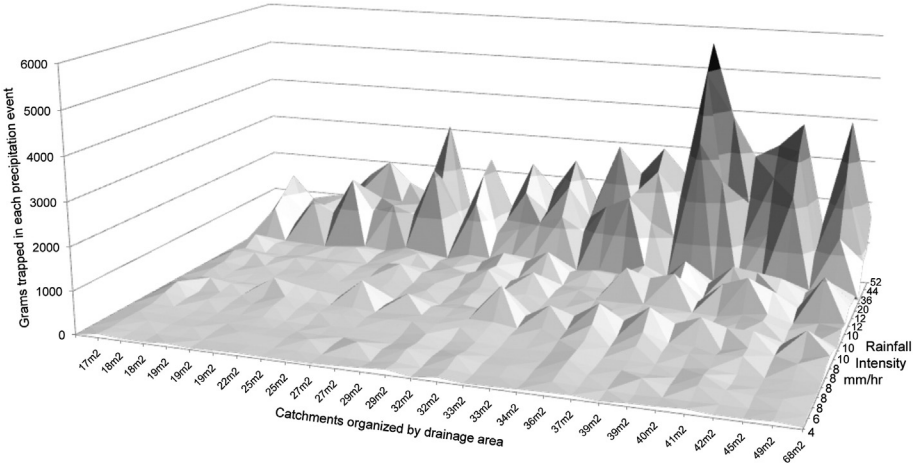

Fig. 8. Plot of grams trapped for all precipitation events with intensities of 4 mm/h or greater. The axis showing the 28 traps is ordered by drainage area in m^2. The axis indicating rainfall intensities is also an ordinal plot — facilitating the visualization of the large jump in detachment that took place with the three highest precipitation intensities. Repetition in units and drainage areas occurs in this diagram, because this plot shows all rain events.

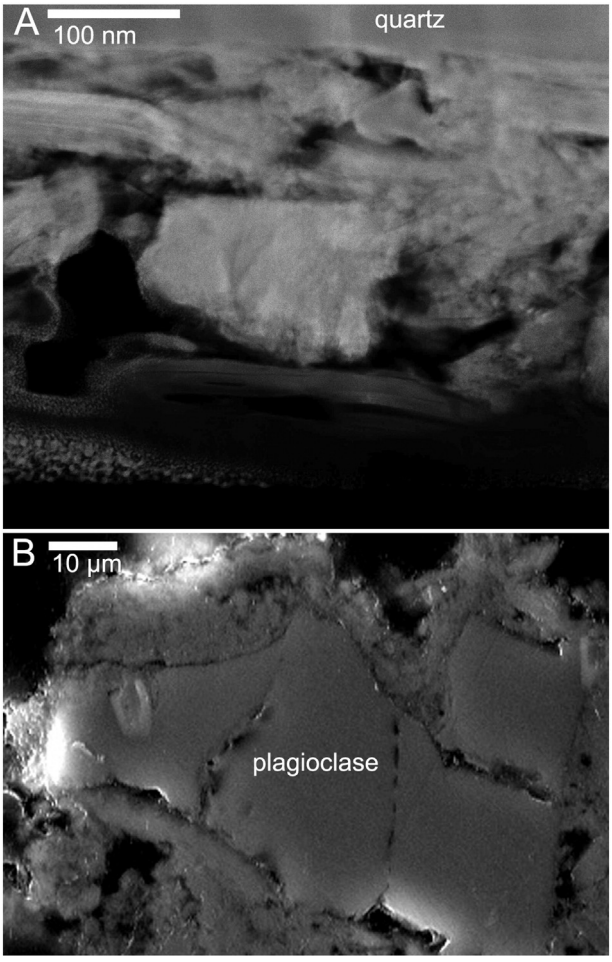

Fig. 9. Anecdotal observation of one detachment event during a 43.6 mm/h precipitation event in a thunderstorm on 8/12/2012. (A) The STEM image is oriented to show the broken surface on the bottom and the center of quartz grus on top; note the chaotic textures of clays and other secondary products having been separated mechanically from the rock. This texture looks like it could be a product shearing. (B) This secondary electron image of the bedrock surface is at a lower magnification, but shows a similarly chaotic texture produced by the detachment event. This image has been oriented so that the detachment surface is at the top.

magnitude precipitation events that promotes ongoing mineral decay and short-distance movement of these decayed particles (Luk et al., 1993; Whitford and Kay, 1999; Neave and Abrahams, 2001).

Despite the fortuitous circumstances of watching and sampling bedrock erosion, most of detachment observed in the field took place on surfaces of bare soil (exposed grus). Then, after the detachment, transport was by interrill overland flow (Parsons et al., 1991) where the rate of erosion is limited by both the rate at which raindrops can "detach sediment of a size that the overflow flow is competent to transport" (p. 143). In the case of the 28 tiny catchments, this was a fairly consistent D_{50} ranging from 1.1 to 1.9 mm (see online supplementary material).

6.2. Suspended sediment generation from crests

Prior research indicates that dust deposition influences the carbonate and silicate fractions of fine particles in Sonoran Desert soils and regolith (Capo and Chadwick, 1993, 1999; Harrison and Dorn, 2014). Thus, there should be no surprise in the result that the suspended sediment sampled exiting three traps originated from dust deposition (Table 1). In other words, the dust appears to be recycling through the geomorphic system — depositing on drainage basins and then – in this case – comprising the suspended sediment load of overland flow.

One implication of the $^{87}Sr/^{86}Sr$ analyses rests in interpreting trap efficiency, since the suspended sediment load derives from "recycled" dust and not local bedrock. Suspended load and perhaps some of the solute load represents eolian additions to the landscape. Another implication rests in recognizing the need to conduct $^{87}Sr/^{86}Sr$ ratio studies of suspended sediment carried by the larger desert washes to assess the importance of dust loading to the overall suspended sediment contribution in larger Sonoran Desert ephemeral streams.

6.3. Erosion rate and vegetation cover

Considering only the grus detached along ridge crests, it is possible to use the average grams of sediment accumulated in each trap (see online supplementary material) to calculate mm/year of erosion in each tiny catchment. The idea is to take average annual grams and "spread" this mass back over each of the 28 drainage areas. Since the density of granite at 2.7 g/cm^3 is equivalent to 370 mm^3/g, product of the trap average (g/year) and granite density (370 mm^3/g) is then divided by the drainage area in mm. The average and standard deviation of the erosion rate of all 28 traps is 0.0310 ± 0.0015 mm/year. When placed in the context of a meta-analysis of modern soil erosion rates across the world (Garcia-Ruiz et al., 2015), the 200 mm/year annual precipitation and 90 mg/km^2 average erosion rate of this study area plots close to the average for global study sites analyzed (Garcia-Ruiz et al., 2015).

Since this study area appears to be reasonably representative of similar arid sites globally, it is interesting to note the similarity of modern erosion rates in this granitic desert setting to geological erosion rates seen in an Ecuadorian Andes montane forest. Prior research established the importance of vegetation cover in reducing erosion rates on arid slopes (Neave and Abrahams, 2001; Wainwright, 2009). A study of natural and human modified erosion rates in the southern Ecuadorian Andes generated a different perspective (Vanacker et al., 2014) that sheds light on the results of this study. In their Fig. 10, Vanacker et al. (2014) plotted "geological erosion rates" as solid squares that center between 0.1 and 0.01 mm/year. In contrast, Vanacker et al. (2014) also analyze erosion rates where anthropogenic activities reduced vegetation cover and accelerated erosion rates. Like the disturbed Ecuadorian Andes sites, the 28 watersheds studied here in a natural setting in the Sonoran Deserts have a low vegetation cover; but while this short-term record does not average a long-enough record to match geological time, it is interesting that the observed erosion rate compares well with

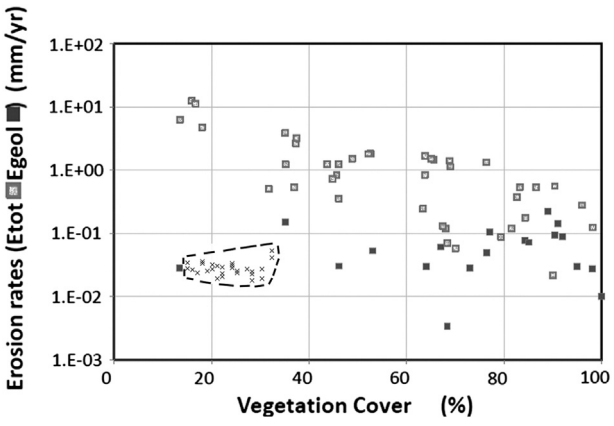

Fig. 10. Erosion rates of the 28 small catchment areas (denoted by the x symbol and within the dashed line) in the arid Sonoran Desert study area of South Mountain plotted on data presented by Vanacker et al. (2014) for the tropical mountain climate of southern part of the Ecuadorian Andes. Dark Squares indicate sites that are felt to be unaffected by the present-day vegetation cover, while light squares indicate sites impacted by modern effects of vegetation reduction. The small x symbols in the lower left portion of the graph are the 28 Sonoran Desert catchments.

the long-term "geological erosion rates" for the southern Ecuadorian Andes.

6.4. Role of rock fragments

Laboratory and simulated rainfall experiments reveal the importance of rock fragments on reducing erosion (Cerdà, 2001) by retarding surface runoff and increasing steady-state infiltration rates. Still, the effect of rock fragments shows tendencies of scale dependence (Poesen et al., 1994), where plots less than a square meter and greater than 100 m^2 see reductions in sediment production from increases in rock fragments. It is in the size range of the drainage basins studied here where the effect of rock fragments is uncertain (Poesen et al., 1994). The same ambiguity of the connection between rock fragments and erosion rates in areas between 10^1 and 10^2 m^2 exists at South Mountain. With an R^2 value of 0.058, the slight positive correlation between more rock cover and higher rates of erosion (Fig. 11) is not statistically significant with a p value of 0.22. A much more robust positive correlation between rock cover and erosion rates occurs on longer granitic slopes in the Mojave Desert studied using ^{137}Cs inventories (Crouvi et al., 2015).

Direct observations during the precipitation results suggest two opposite processes related to rock fragments. Erosive effects derive from bedrock channeling runoff and enhancing grain detachment through the development of a horseshoe vortex where water pours off bedrock surfaces. On the other hand, bare rock surfaces also funnel runoff to the roots of perennial plants — suggesting that the plants successfully germinated at these more favorable locations. Plant growth in turn promotes lower erosion rates. Thus, this research supports the observations of Crouvi et al. (2015) on the importance of rock fragments on arid slopes and also that of Poesen et al. (1994) that scale is important in considering different processes.

One perplexing aspect of the full data set (see online supplementary material) rests in the detachment and transport of some sediment with small rainfall amounts of 3 mm to 7 mm. Field observations during these minor precipitation events reveals only infiltration into soil and plant canopy. The only runoff from these small rains occurred in association with rock surfaces. It was possible to watch the runoff channel on bare rock and move grus off the rock surfaces. Thus, a speculative notion is that this "rock face washing" could be responsible for the grus moved during small rains, where rock face washing can be set up by prior intense rains, moving grus onto bare rock surfaces. When flow ceases after the intense rain, some grus remains on bare rock surfaces. Then, minor rains generate sufficient flow over rock surfaces to transport some grus into the sediment traps.

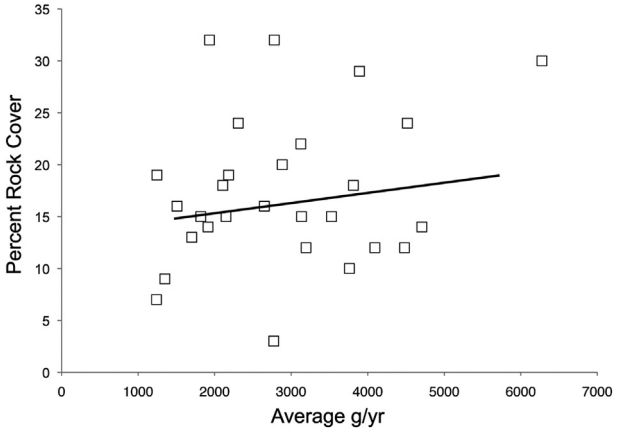

Fig. 11. Linear regression of percent rock cover and the average grams of sediment eroded from the 28 catchments at South Mountain. This regression is not statistically significant (p value of 0.22 and R^2 value of 0.058).

7. Conclusion

Traps collected sediment detached from 28 drainages with areas ranging from 18 to 68 m^2 along the crest of an arid Sonoran Desert granitic range. Data gathered consist of grams of sediment detached by every precipitation event over a period of 3 years, the average slope of each watershed, the canopy of perennial vegetation, the percent of exposed bedrock, the percent of exposed soil, the D_{50} of trapped particles, rainfall recorded in a nearby automated rain gage, and $^{87}Sr/^{86}Sr$ ratios for suspended sediment flowing out of the traps and dust falling on slope surfaces.

The three-year time period of observation included two extreme rain events — a 1000-year precipitation event from an August thunderstorm and a 500-year event from remnant hurricane moisture. The mass trapped by these two events and a third 100-year thunderstorm was almost twice all of the other precipitation events combined, with the ratio averaging 1.79 ± 0.54 for all drainages.

Data from the 28 traps indicate that more exposed soil, larger drainage areas, and steeper slopes all promote erosion. No transport took place during rain events of 2 mm or less, and only minimal erosion occurred during events between 3 and 7 mm associated with washing grus off bare rock surfaces. Rains with precipitation intensities of 36 mm/h or more result in a big jump in grus detachment and transport. Although trap data are limited to just bedload, $^{87}Sr/^{86}Sr$ ratios indicate that the suspended sediment departing the traps derive from eolian dust and not the underlying bedrock.

Considered from a perspective of erosion rates averaged over a three-year period, the trapped grus amount to a rate of 0.0310 ± 0.0015 mm/year. These rates correspond to values seen in the Ecuadorian Andes over geological timescales, even though they occurred in the Sonoran Desert with minimal vegetation cover. Considered from the perspective of the role of rock fragments, no clear relationship exists between the percent of rock cover and erosion rates where rocks shedding overland flow can both accelerate and decrease erosion through different processes.

Acknowledgments

I would like to thank the City of Phoenix for permission to carry out this research.

Appendix A. Supplementary data

Supplementary data to this article can be found online at http://dx.doi.org/10.1016/j.geomorph.2015.08.017.

References

Brazel, A.J., 1989. Dust and climate in the American southwest. Paleoclimatology and Paleometeorology: Modern and Past Patterns of Global Atmospheric Transport. Kluwer Academic Publishers, Dordrecht.
Capo, R.C., Chadwick, O.A., 1993. Application of strontium isotopes to the mass balance of calcium in desert soils: eolian input vs in situ weathering. Geol. Soc. Am. Abstr. Prog. 25 (6), A394.
Capo, R.C., Chadwick, O.A., 1999. Sources of strontium and calcium in desert soil and calcrete. Earth Planet. Sci. Lett. 170, 61–72.
Capo, R.C., Stewart, B.A., Chadwick, O.A., 1998. Strontium isotopes as tracers of ecosystem processes: theory and methods. Geoderma 82, 197–225.
Cerdà, A., 2001. Effects of rock fragment cover on soil infiltration, interrill runoff and erosion. Eur. J. Soil Sci. 52, 59–68.
Coney, P.J., Harms, T.A., 1984. Cordilleran metamorphic core complexes: Cenozoic extensional relics of Mesozoic compression. Geology 12, 550–554.
Coppus, R., Imeson, A.C., 2002. Extreme events controlling erosion and sediment transport in a semi-arid sub-Andean valley. Earth Surf. Process. Landf. 27, 1365–1375.
Crouvi, O., Polyakov, V.O., Pelletier, J.D., Rasmussen, C., 2015. Decadal-scale soil redistribution along hillslopes in the Mojave Desert. Earth Surf. Dyn. 3, 251–264. http://dx.doi.org/10.5194/esurf-3-251-2015.
David-Novak, H.B., Morin, E., Enzel, Y., 2004. Modern extreme storms and the rainfall thresholds for initiating debris flows on the hyperarid western escarpment of the Dead Sea, Israel. Geol. Soc. Am. Bull. 116, 718–728.

Dick, G.S., Anderson, R.S., Sampson, D.E., 1997. Controls on flash flood magnitude and hydrograph shape, Upper Blue Hills badlands, Utah. Geology 25, 45–48.
Dorn, R.I., 1995. Digital processing of back-scatter electron imagery: a microscopic approach to quantifying chemical weathering. Geol. Soc. Am. Bull. 107, 725–741.
Ehlen, J., 1999. Fracture characteristics in weathered granites. Geomorphology 31, 29–45.
Ehlen, J., 2005. Above the weathering front: contrasting approaches to the study and classification of weathered mantle. Geomorphology 67, 7–21.
Ehlen, J., Wohl, E., 2002. Joints and landform evolution in bedrock canyons. Trans. Jpn. Geomorphol. Union 23–2, 237–255.
Erpul, G., Gabriels, D., Norton, L.D., 2005. Sand detachment by wind-driven raindrops. Earth Surf. Process. Landf. 30, 241–250.
Furbish, D.J., Childs, E.M., Haff, P.K., Schmeeckle, M.W., 2009. Rain splash of soil grains as a stochastic advection–dispersion process, with implications for desert plant-soil interactions and land-surface evolution. J. Geophys. Res. 114, F00A03. http://dx.doi.org/10.1029/2009JF001265 (18 pp.).
Garcia-Ruiz, J.M., Beguería, S., Nadal-Romero, E., Gonzalez-Hidalgo, J.C., Lana-Renault, N., Sanjuán, Y., 2015. A meta-analysis of soil erosion rates across the world. Geomorphology 239, 160–173.
Harrison, E.J., Dorn, R.I., 2014. Introducing a terrestrial carbon pool in warm desert bedrock mountains, Southwestern USA. Glob. Biogeochem. Cycles 28, 253–268.
Harvey, A.M., 2006. Geomorphological response to an extreme flood: a case from southeast Spain. Earth Surf. Process. Landf. 9, 267–279.
Holt, W.E., Chase, C.G., Wallace, T.C., 1986. Crustal structure from 3-dimensional gravity modeling of a metamorphic core complex — a model for uplift, Santa Catalina-Rincon Mountains, Arizona. Geology 14 (11), 927–930.
Lekach, J., Schick, A.P., 1983. Evidence for transport of bedload in waves: analysis of fluvial sediment in a small upland stream channel. Catena 10, 267–279.
Luk, S.H., Abrahams, A.D., Parsons, A.J., 1993. Sediment sources and sediment transport by rill flow and interrill flow on a semi-arid piedmont slope, southern Arizona. Catena 20, 93–111.
Marcus, M.G., Brazel, A.J., 1992. Summer dust storms in the Arizona Desert. In: Janelle, D.G. (Ed.), Geographical Snapshots of North America. Guilford Press, New York, pp. 411–415.
Mather, A.E., Hartley, A., 2005. Flow events on a hyper-arid alluvial fan: Quebrada Tambores, Salar de Atacama, northern Chile. In: Harvey, A.M., Mather, A.E., Stokes, M. (Eds.), Alluvial Fans: Geomorphology, Sedimentology, Dynamics. Geological Society of London, London, pp. 9–29.
Moharana, P.C., Kar, A., 2010. Quantitative measurement of arid fluvial processes: results from an upland catchment in Thar Desert. J. Geol. Soc. India 76, 86–92.
Nations, D., Stump, E., 1981. Geology of Arizona. Kendall Hunt, Dubuque.
Neave, M., Abrahams, A.D., 2001. Impact of small mammal disturbances on sediment yield from grassland and shrubland ecosystems in the Chihuahuan Desert. Catena 44, 285–303.
Osterkamp, W.R., Friedman, J.M., 2000. The disparity between extreme rainfall events and rare floods — with emphasis on the semi-arid American West. Hydrol. Process. 14, 2817–2829.
Parsons, A.J., Abrahams, A., Luk, S.H., 1991. Size characteristics of sediment in interrill overland flow on a semiarid hillslope, Southern Arizona. Earth Surf. Process. Landf. 16, 143–152.
Parsons, A.J., Stromberg, S.G.L., Greener, M., 1998. Sediment-transport competence of rain-impacted interrill overland flow. Earth Surf. Process. Landf. 23, 365–375.
Phillips, J.D., 2014. Thresholds mode switching, and emergent equilibrium in geomorphic systems. Earth Surf. Process. Landf. 39, 71–79.
Pickup, G., 1991. Event frequency and landscape stability on the floodplain systems of arid Central Australia. Quat. Sci. Rev. 1991, 463–473.
Poesen, J.W., Torri, D., Bunte, K., 1994. Effects of rock fragments on soil erosion by water at different spatial scales: a review. Catena 23, 141–186.
Puigdefabregas, J., del Barrio, G., Boer, M.M., Gutierrez, L., Sole, A., 1998. Differential responses of hillslope and channel elements to rainfall events in a semi-arid area. Geomorphology 23, 337–351.
Reheis, M.C., Kihl, R., 1995. Dust deposition in southern Nevada and California, 1984–1989: relations to climate, source area, and source lithology. J. Geophys. Res. 100, D8893–D8919.
Reynolds, S.J., 1985. Geology of the South Mountains, central Arizona. Ariz. Bur. Geol. Miner. Technol. Bull. 195.
Richards, K.S., Brooks, S.M., Clifford, N.J., Harris, T.R.J., Lane, S.N., 1995. Theory, measurement and testing in "real" geomorphology and physical geography. In: Stoddart, D. (Ed.), Process and Form in Geomorphology. Blackwell, Oxford, pp. 265–292.
Schick, A.P., 1988. Hydrologic aspects of floods in hyper-arid environments. In: Baker, V.R., Kochel, R.C., Patton, P.C. (Eds.), Flood Geomorphology. Wiley Interscience, New York, pp. 189–203.
Shaw, P.A., Thomas, D.S., Nash, D.J., 1992. Late quaternary fluvial activity in the dry valleys (mekgacha) of the Middle and Southern Kalahari, southern Africa. J. Quat. Sci. 7, 273–281.
Spencer, J.E., 1984. The role of tectonic denudation in warping and uplift of low-angle normal faults. Geology 12, 95–98.
Tomlinson, E., Kappel, B., Muhlestein, G., Hultstrand, D., Parzybok, T., 2013. Probable Maximum Precipitation Study for Arizona. Applied Weather Associates, Monument, CO.
Twidale, C.R., 1982. Granite Landforms. Elsevier, Amsterdam.
Vanacker, V., Bellin, N., Molina, A., Kubik, P.W., 2014. Erosion regulation as a function of human disturbances to vegetation cover: a conceptual model. Landsc. Ecol. 29, 293–309.
Wainwright, J., 2009. Desert ecogeomorphology. In: Parsons, A.J., Abrahams, A.D. (Eds.), Geomorphology of Desert Environments, 2nd ed. Springer, Amsterdam, pp. 21–66.
Whitford, W.G., Kay, F.R., 1999. Biopedturbation by mammals in deserts: a review. J. Arid Environ. 41, 202–230.